ChemComm

View Article Online / Journal Homepage / Table of Contents for this issue
Dynamic Article Links

Cite this: *Chem. Commun.*, 2012, **48**, 1201–1217

www.rsc.org/chemcomm

FEATURE ARTICLE

Enhancing the performances of Li-ion batteries by carbon-coating: present and future

Huiqiao Li and Haoshen Zhou*

Received 2nd August 2011, Accepted 28th September 2011
DOI: 10.1039/c1cc14764a

With progress of knowledge of electrode materials, it has been found that their surface structures are of great importance to the electrochemical performance of Li-ion batteries. Carbon coating can effectively increase the electrode conductivity, improve the surface chemistry of the active material, and protect the electrode from direct contact with electrolyte, leading to enhanced cycle life of the batteries. Carbon coating together with nanotechnology provides good conductivity as well as fast Li-ion diffusion, and thus also results in good rate capabilities. The recent development of carbon coating techniques in lithium-ion batteries is discussed with detailed examples of typical cathode and anode materials. The limitation of current technology and future perspective of the new concept of "hybrid coating" are also pointed out.

1. Introduction

Li-ion batteries (LIB) have dominated the portable electronic markets during the past 2 decades because of their much higher energy per unit weight or volume compared to other rechargeable battery systems. Now, they are being intensively persued for transportation applications in hybrid electric vehicles (HEV), plug-in hybrid electric vehicles (PHEV), and electric vehicles (EV), as well as seriously considered for stationary storage and utilization of intermittent renewable energies like solar and wind. The success of lithium ion technology for these ongoing large-scale applications will depend largely on the cost, safety, cycle life, charge/discharge rates, energy and power, which are in turn controlled by the component materials used in the batteries.[1,2] Although tremendous efforts have been made to use new materials in both cathodes and anodes, only several materials among them achieved

---

Energy Technology Research Institute, National Institute of Advanced Industrial Science and Technology (AIST), Umezono 1-1-1, Tsukuba, 305-8568, Japan. E-mail: hs.zhou@aist.go.jp; Fax: +81-29-8613489; Tel: +81-29-8615795

Huiqiao Li

Huiqiao Li received her BSc degree in Chemistry from Zhengzhou University in 2003, and then received her PhD degree in Physical Chemistry from Fudan University in 2008, P. R. China. Currently, she works as a postdoctoral fellow in Dr Haoshen Zhou's group at Energy Technology Research Institute, National Institute, National Institute of Advanced Industrial Science and Technology (AIST), Japan. She has authored and co-authored over 20 refereed journal publications. Her research interests include energy storage materials and devices as lithium-ion batteries and supercapacitors.

Haoshen Zhou

Haoshen Zhou graduated from the Department of Physics, Nanjing University, China, 1985. He obtained his PhD degree from the Department of Chemical Engineering, The University of Tokyo, Japan, 1994. He is now the leader of the Energy Interface Technology Group, Energy Technology Research Institute, National Institute of Advanced Industrial Science and Technology (AIST), Japan. He is also the guest professor in both University of Tokyo and Nanjing University. His research interests include the synthesis of nanostructure functional materials and their applications in lithium ion batteries, metal–air batteries, new type batteries/cells, fuel cells, dye sensitized solar cells, hydrophobic/hydrophilic surfaces, electrochemical sensors and optical waveguide gas sensors.

the commercial utilization due to the critical criteria of an industrial battery product.

The biggest challenge is that Li-ion batteries are complicated devices whose components never reach thermodynamic stability.[3] The poor cell lifetimes are rooted mainly in side reactions occurring at the electrode–electrolyte interface. Thus, mastering the chemical stability of any new electrode material with respect to its operating electrolyte medium, which requires a control of the electrode–electrolyte interface through surface chemistry, is as important as designing new materials.[4] Obviously, optimizing an electrode material is the first step in the process leading to its implementation in a practical cell. It has turned out that surface coating is an economic and feasible technology to improve the battery performances by virtue of modifying the surface chemistry or providing protection layers to minimize the direct contact of the active material with the electrolyte. By smartly selecting the coating materials such that the coating layers are capable of improving the ionic or electronic conductivity, suppressing phase transition, increasing structural stability, decreasing the disorder of cations in crystal sites, reducing transition metal dissolution, acting as a HF scavenger to reduce the electrolyte acidity, favoring the formation of solid–electrolyte-interface (SEI) film on the anode surface, and so on, electrode resistance, side reactions and heat generation during cycling are decreased, which consequently leads to a remarkable improvement in cycle life, rate capability, reversible capacity, coulomb efficiency of the first cycle, and overcharge tolerance *etc.*[5–8] The coating materials investigated to date include various carbon, metal oxides (Al_2O_3, ZrO_2, ZnO, MgO, SiO_2, TiO_2, CeO_2), metal phosphate ($AlPO_4$), metal fluoride (AlF_3), metal oxyfluoride (BiOF), glass composite (Li_2O–$2B_2O_3$), *etc.*, among which carbon coating plays an exclusive role for anode materials as well as a more and more important role in new generation cathode materials, due to the multi-functional advantages arising from the unique chemical and physical properties of carbon. Therefore, we intend to focus our introduction on carbon coating techniques in several typical types of electrode materials for both cathodes and anodes. In the end, we also noted the challenges faced by the current coating technology and proposed a new concept of "hybrid coating" (multi-components coating) for the future to address the limitation of the present single-component coating layer.

2. The motivation to use carbon coatings

2.1 Excellent electrical conductivity

The most important superiority of carbon to other coating materials is that it is a good electronic conductor. We know that the power ability ($P = U \times I$, U is the cell voltage and I is the current density) of a battery is critically determined by its internal resistance (R): higher resistance leads to a more rapid decline of the cell voltage at elevated current density due to the ohmic drop (namely the deviation between practical and theoretical voltage, $\Delta U = I \times R$). In addition, the generated heat (Q) accompanied with the charge/discharge process, the reason of the temperature increase within the battery, would grow with the square of internal resistance according to the ohmic law ($Q = I \times R^2$). Higher working temperature would accelerate the degradation of the battery life. For an established electrode, the total internal resistance (R) is the sum of electrical resistance (R_e), ionic resistance (R_i) and interfacial resistance (R_{in}).[9] Since most of the electrode active materials are semiconductors or insulators and synthesized as powder, the practical electrodes are actually composites which usually contain an active material, a conductive additive to endow necessary electrical conductivity, and a polymer binder to hold the mix together and bond the mix to the conductive collector. The general sources of each type of resistance are given in Table 1.[9]

Table 1 Internal resistance of an electrode in a cell. Ref. 9, Copyright 2010 Elsevier

Resistance type	Internal resistance of a cell ($R = R_i + R_e + R_{in}$)
Ionic (R_i)	Electrode active particle Electrolyte
Electrical (R_e)	Electrode active particle Conductive additives Percolation network of additives in electrode Current collectors Electrical taps
Interfacial (R_{in})	Between electrolyte and electrodes Between electrode active particles Between electrode particles and conductive additives Between conductive and additives and current collector

Examining the sources of resistance can provide insight into the key barriers to optimized conduction in electrochemical cells. Upon charging/discharging, the electrode undergoes the volume insertion/deinsertion of Li ions into/from the active particles, which involves the diffusion and conduction of both Li ions and electrons. It is known that the active material shows much lower ionic conductivity than the electrolyte as well as much poorer electrical conductivity than the carbon black or acetylene black additives. So, the electrode resistance is mainly determined by (a) the ionic and electronic resistance of active particles and (b) the interfacial resistances from the electrolyte/electrode interface and particle/particle boundaries.

Suppose the composite electrode was perfectively made, by which the electrolyte can well penetrate into the pores of the electrode and surround the active particles; the conductive additives are made of small particles and homogeneously dispersed within the whole electrode so that each of the active particle will be "point-contacted" by one or more tiny additive particles. If the electronic conductivity inside bulk active particles is much lower than the ionic conductivity, the ambipolar (ionic and electronic) diffusion can only start at the vicinity of point contact, which leads to a constrained electric field around this point, as shown in Fig. 1a.[10] If the electron conductivity is much higher than the ionic, *e.g.* graphite, the electrons will spread around the particle's surface which will form active double layers of active ions and electrons, and cause ambipolar diffusion into and out of bulk particles, as shown in Fig. 1b. If the active particle is coated by a thin layer of carbon, the coating supplies fast electrons and can be also permeable for Li^+ ions from the surrounding electrolyte solution. This approach ensures the effective ambipolar diffusion

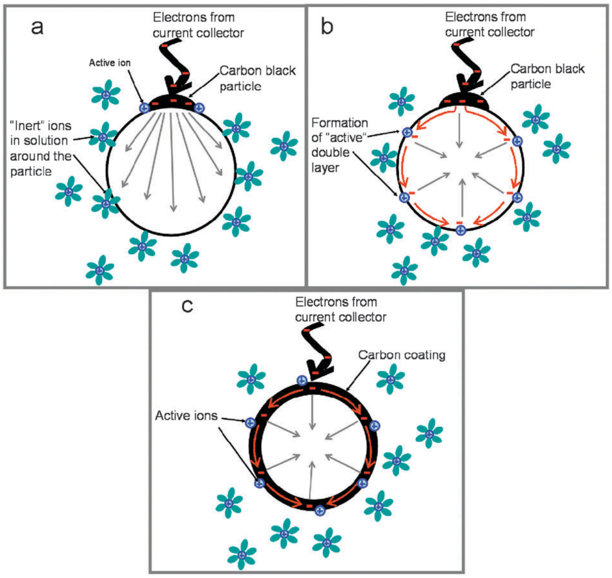

Fig. 1 Schematic conduction/diffusion of electron and Li ions within a single active particle by point-contact with tiny additive particles or by full-contact with a carbon-coating layer: (a) the electronic conductivity is much lower than the ionic conductivity, (b) the ionic conductivity is much lower than the electronic conductivity, (c) the case of perfect carbon-coating regardless of electronic and ionic conductivity. Ref. 10, Copyright 2007 Elsevier.

of Li^+ and e^- into/out of active particles (as indicated by arrows in Fig. 1c) regardless of particle conductivity.[10]

The first generation LIB employs electrode materials composed of millimetre particles, it is a low-power device (slow charge/discharge). An increase in the charge/discharge rate of LIB of more than one order of magnitude is required to meet the future demands of hybrid electric vehicles and clean energy storage. No matter how creative we are in designing new lithium intercalation hosts with higher rates, limits exist because of the intrinsic slow diffusivity of lithium ions in the solid state (*ca.* 10^{-8} cm^2 s^{-1}). Nanostructures have a genuine potential to make a significant impact on the rate capability of LIB due to the fact that the distance over which Li^+ must diffuse in the solid state dramatically decreases with the reduced particle size.[11] However, the nanosized particles tend to form agglomerates due to the high surface energy arising from high surface area, which make them difficult to disperse and mix with conductive additives, as shown in Fig. 2a.[12] Accordingly, the electronic transport length (L_e) is still much larger than the particle size (r) because only a small amount of nanoparticles in the agglomerates can directly contact the carbon additive and obtain electrons. Furthermore, the interfacial resistance would be much higher due to the largely increased particle/particle boundary resistance. If each nanoparticle is fully coated with an electronic conductive layer, the electronic transport length (L_e) would be effectively shortened to a level comparable to (or less than) the particle size (r) of the nanomaterials, as shown in Fig. 2b.[12] The electrons can pass along the outer surface of each nanoparticle, forming a continuous transport path in the whole electrode, thus leading to much reduced particle/particle interface resistance. Besides profiting from the good electrical conductivity endowed by the carbon coating layer, the amount of the conductive additive can be decreased, which equals a higher active material loading and energy density in the full-size battery.

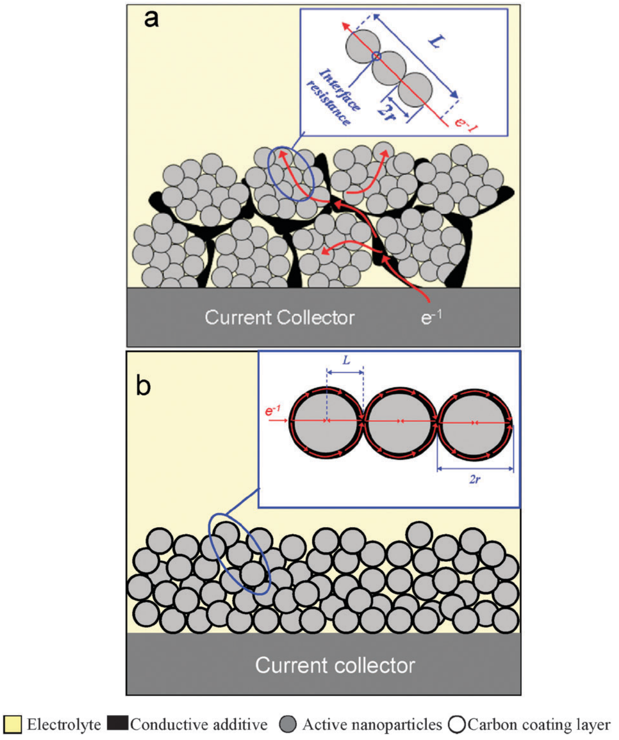

Fig. 2 Schematic representation of the electronic transport length (L_e) in a nanoparticle based electrode: (a) without carbon coating; (b) with carbon coating. Ref. 12, Copyright 2010, The Royal Society of Chemistry.

2.2 Superior chemical and electrochemical stability

It is a great challenge to develop a battery chemistry that can meet the 15 year calendar life requirement for transportation applications. The charged electrode materials, whether delithiated cathode or lithiated anode, tend to react with the nonaqueous electrolyte violently at elevated temperatures. These energetically favored side reactions can also occur slowly at ambient temperature, resulting in slow degradation of electrode materials and, consequently, battery performance.[8] The cathode materials may amplify or even catalyze the decomposition of the electrolyte if their operation voltages exceed the electrochemical resistance of the electrolyte oxidation.[4] As for electrolyte, the dominant lithium salt $LiPF_6$ is sensitive to a trace amount of moisture. The produced HF by its hydrolysis would cause the dissolution of the transition metals and erode the surface of active materials (Fig. 3a), which also lead to capacity decay upon long term cycling. Carbon material has a wide electrochemically stable window in organic electrolytes. It shows electrochemical activity towards the electrolyte only at very low potential and will not oxidize even up to a high cutoff of the cell voltage, and thus can be applied as the coating material for a wide range of electrode materials. Carbon also has a very good chemical stability, and thus promises good resistance to HF corrosion (Fig. 3b). Common coating materials, such as metal oxides, are capable of diffusing into the crystal lattice of

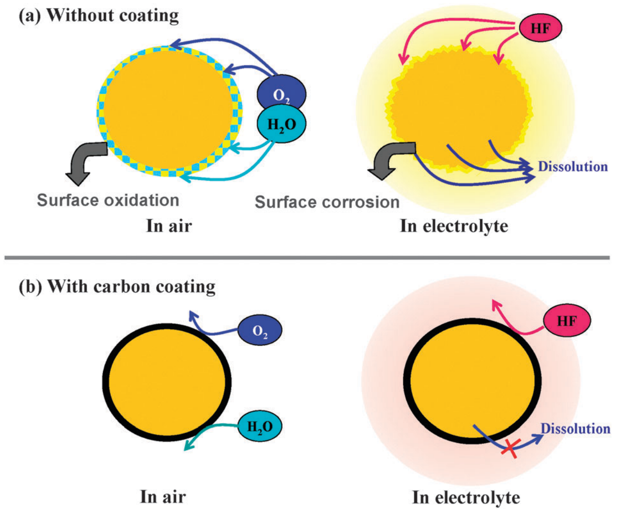

Fig. 3 Schematic illustration showing the long-term degradation of active material in air and in electrolyte without (a) and with (b) the protective coating layer.

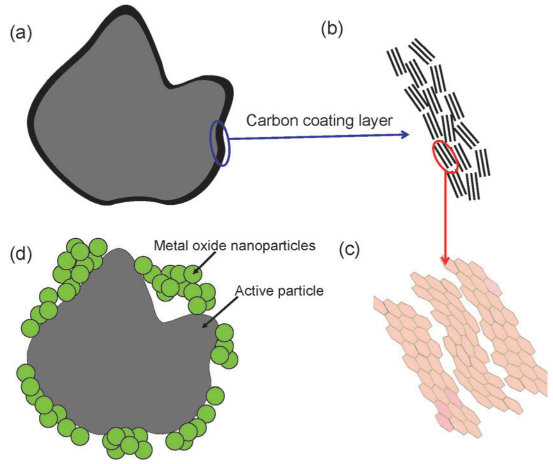

Fig. 4 Schematic illustration showing different adaptability of the carbon coating (a) and metal oxide coating (d) to the geometry of the substrate material. (b) and (c) showing more details of the carbon coating layer.

the active material and substitute the active elements when treated at high temperature for long term; while carbon coating just affects the surface of the active material. In terms of some low-valence active materials, *e.g.* $LiFePO_4$ and VO_2, they may undergo gradual surface oxidation when exposed to air during long-term storage (Fig. 3a), especially in the case of nanomaterial with a high surface area. If coated by carbon, such active material will be prevented from contact with the oxygen and moisture in the air, and as a result, the surface degradation in air shown in Fig. 3b will be greatly retarded. Attributed to the superior chemical and electrochemical stability, the carbon coating layer can act as a good protecting layer which not only retards the degradation of active material during storage but also slows down the capacity fading upon charge/discharge cycling.

2.3 Unique physical properties

Carbon is known to have many allotropes, such as graphite, amorphous (actually nanosized graphite crystallites), diamond, carbon nanotube, graphene, fullerene *etc.*, due to its versatile bonding constructions derived from sp, sp^2, sp^3 hybrid orbitals as well as p–p π orbitals. Accordingly, it possesses many unique physical properties, *e.g.*, anisotropic conductivity, low density, high mechanical strength, structural flexibility, and so on. When used as the coating material, it easily forms a thin film layer on the surface of the active material by chemical vapor deposition or *in situ* pyrolysis of the organic precursors, as shown in Fig. 4a. The adhesion of carbon on the surface is possible because of the fact that the carbon chooses the structure of deposit in the form of amorphous carbon (nanosized graphite crystallites, Fig. 4b) which leads to a small hardness (10 GPa), allowing the film to adjust the surface roughness and the curvature of the active particles.[13] The more general sp^2 bonding prefers a layer-by-layer assembly of hexagonal atom planes, providing efficient electronic conductivity, as shown in Fig. 4c. Besides, the ionic transport from the electrolytic medium to the core of active particles is ensured by the diffusion of Li ions throughout the micropores of the coating layer (the interspace between disoriented nano-crystallites in Fig. 4b). In comparison, the metal oxide coating layers are composed of nanoparticles with which it is difficult to form a uniform thin layer due to their self-agglomeration and poor flexibility to geometry, as shown in Fig. 4d.

For nanosized active materials, the carbon coating layer can play a positive role in maintaining the nanomorphology. The preparation of many active materials involves the calcination process at high temperature (700–1000 °C) to obtain required high crystallization, however, such calcination would cause rapid size growth and serious morphology deterioration. During calcination, the full carbon coating layer works as a solid barrier between active particles, preventing them from sintering to large particles.

In addition, the carbon coating layer can also serve as an elastic shell to accommodate the volume changes of the active material upon Li insertion/de-insertion, circumventing the peeling-off of active material from the current collector due to cracking and pulverization.[14]

2.4 Low cost

Carbon is one of the most abundant elements in the earth. Various sources of low cost and wide availability, such as sugar, resin, pitch, polymer, and hydrocarbon, can be used as the carbon precursors. Carbon coatings on the surface of active material can be easily realized by chemical vapor deposition, sol–gel coating of the precursor and then thermal decomposition of the carbon sources at high temperature. These processes are simple and need no expensive equipment. The properties of the coating layer, *e.g.* conductivity and thickness, can also be conveniently adjusted by carbon content, pyrolysis temperature and duration time. So carbon coating is one of the most widely used technologies in lithium-ion batteries.

3. Carbon coatings for cathode materials

3.1 $LiMPO_4$

There is intensive research activity into alternative electrode materials for the next generation of rechargeable lithium-ion batteries for use in HEV. Olivine-structured orthophosphates $LiMPO_4$ (M = Mn, Fe, Co and Ni) have been proposed as viable alternatives because of their low cost, excellent cycle life, and thermal stability. The existence of an $M_n(PO_4)_y$ framework provides an excellent stability and long term cycling to this type of cathode in comparison to lithium transition metal oxides. The oxygen–phosphorous bond is more covalent in nature than polar oxygen–metal bonds. Thus, no loss of oxygen occurs from the framework and the reactivity with the electrolyte is low.[15] However, the main difficulty in using this family of materials is that they have intrinsically poor electronic and ionic conductivity. Typically, this is overcome through a combination of reducing the particle size and surface coating of an electronically conductive phase such as carbon. Surface carbon coating effectively alleviates the problem of low electronic conductivity, while small particle size would reduce the diffusion length for the reaction with lithium, leading to increase of the rate capability of $LiMPO_4$ cathode materials by several orders of magnitude. In fact, the use of thin carbon coating has become a critical component for $LiMPO_4$ species and is mandatory for their operation at high rates, due to the poor intrinsic transport properties of these powders. As envisioned by Tarascon *et al.*, for any insulating insertion compound there is a threshold crystallite size beyond which the material could be used as an electrode, if electrons can be provided through effective coating techniques.[16]

$LiFePO_4$, being environmentally benign and showing high safety, attracted the most research attention and has been brought to a practical level of commercial usage. The $LiFePO_4$ operates at a flat voltage of 3.4 V *vs.* Li^+/Li, yields a theoretical specific capacity of 170 mA h g^{-1}, and a theoretical gravimetric energy density comparable to that of $LiCoO_2$. However, the pristine form of $LiFePO_4$ has an electronic conductivity of only 10^{-9}–10^{-10} S cm^{-1}, several orders of magnitude lower than those of $LiCoO_2$ (10^{-4} S cm^{-1}) and $LiMn_2O_4$ (10^{-4} S cm^{-1}), and exhibits very poor rate performance. Over the recent years, much effort has been made to improve the rate performance of $LiFePO_4$ by carbon coating to increase the conductivity or using low-temperature routes to obtain tailored particles. By simple carbon coating, a much higher conductivity ($>10^{-4}$ S cm^{-1}) can be achieved for the $LiFePO_4$/C composites.[17–20] However, these carbon-coated $LiFePO_4$ particles are generally prepared by thermal decomposition of carbon-containing precursors, which tends to produce $LiFePO_4$ particles with a partial coating of carbon. Moreover, the high temperature process, which is needed to ensure a high conductivity of the resulting carbon, easily caused the growth of the $LiFePO_4$ crystallites. If $LiFePO_4$ can be made in nanosize and with uniform surface carbon coating, the utilization of its theoretical capacity at even high rates would be possible.

In 2008, a novel strategy based on an *in situ* polymerization restriction method was reported to synthesize $LiFePO_4$ nanoparticles (20–40 nm) with a full coating of a thin carbon layer (1–2 nm in thickness), as shown in Fig. 5a–c.[21] The strategy included one *in situ* polymerization reaction and two typical restriction processes (Fig. 5d): when Fe^{3+} was added in the solution containing PO_4^{3-} and aniline, the white $FePO_4$ deposits were first formed. The Fe^{3+} on the outer surface of fresh $FePO_4$ deposits would oxidize the aniline to initiate its *in situ* polymerization, thus forming a green polyaniline (PANI) shell to restrict the size growth of $FePO_4$ deposits. The prepared $FePO_4$–PANI composite was combined with lithium salt and some sugar to produce $LiFePO_4$–carbon core–shell nanoparticles by heat treatment at 700 °C under an Ar atmosphere with 5% H_2, during which, the polymer

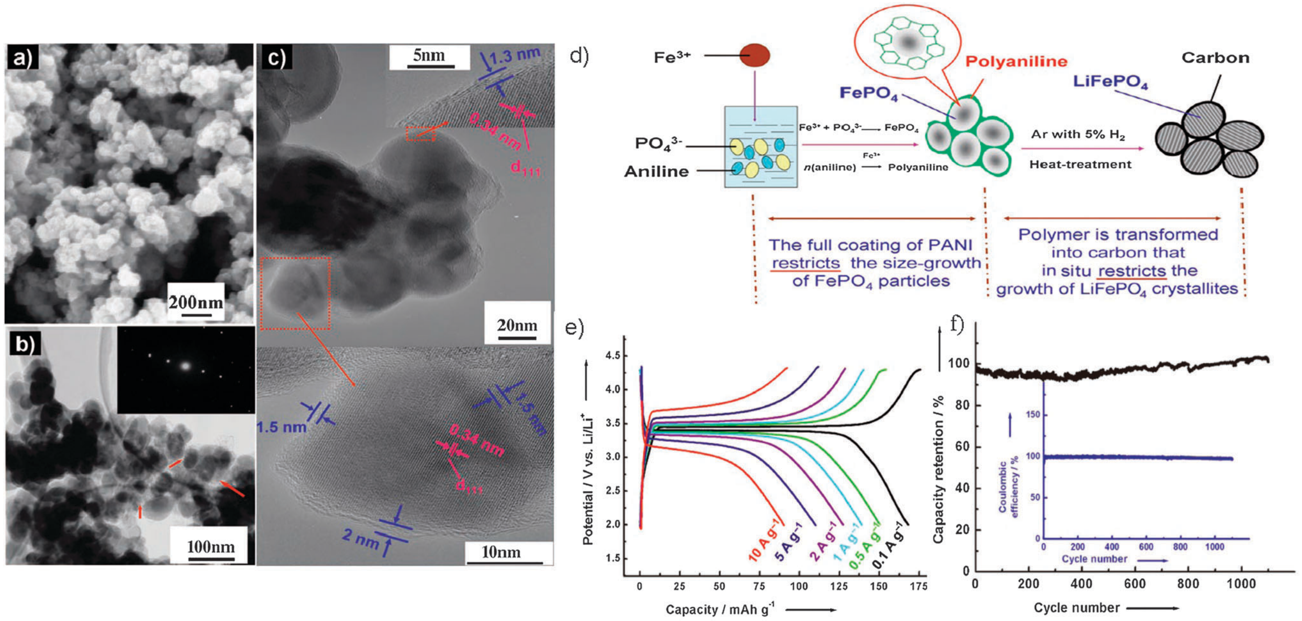

Fig. 5 SEM (a) and TEM (b, c) images of the $LiFePO_4$/carbon nanoparticles with a core–shell structure obtained by an *in situ* polymerization restriction strategy; (d) preparation process for the core–shell $LiFePO_4$/carbon nanocomposite including an *in situ* polymerization reaction and two restriction processes; (e) rate performance and (f) cycle life (tested at a current density of 0.1 A g^{-1}) of the prepared core–shell $LiFePO_4$/carbon nanocomposite. Ref. 21, Copyright 2008, Wiley-VCH.

shell was transformed into a thin carbon layer that *in situ* restricted the crystallite growth of $LiFePO_4$. Such a core–shell structured $LiFePO_4$/carbon nanocomposite achieved a high reversible capacity (168 mA h g^{-1}) at a current density of 0.1 A g^{-1} (about 0.6C), nearly the theoretical value of $LiFePO_4$. Even at a high charge/discharge rate of 60C (10 A g^{-1}), this material still delivered a capacity of 90 mA h g^{-1} (Fig. 5e). The high power performance profits from both the enhanced electron transport by full carbon coating and the much decreased diffusion length for Li ions by reduction of the particle size. Furthermore, it also exhibited an excellent cycling performance, with less than 5% discharge capacity loss over 1100 cycles (Fig. 5f). Recently, graphene has also been considered as a new type of carbon coating source for high power $LiFePO_4$ material due to its unique properties such as high conductivity and superior structural flexibility. The graphene-modified $LiFePO_4$ composite was prepared from $LiFePO_4$ nanoparticles and graphene oxide nanosheets by spray-drying and annealing processes. The obtained composites are made of 2–5 μm quasi-spherical secondary microparticles in which the $LiFePO_4$ primary nanoparticles are wrapped homogeneously and loosely in a graphene 3D network.[22] Such nanostructure facilitates electron migration throughout the secondary particles, while the presence of abundant voids between the $LiFePO_4$ nanoparticles and graphene sheets is beneficial for Li^+ diffusion, thus the composite cathode could exhibit a high rate performance, *e.g.*, 70 mA h g^{-1} at 60C discharge rate, and a capacity decay rate of $<15\%$ for 1000 cycles.

Obviously, the carbon coatings help to obtain a long cycle life of $LiFePO_4$, as given in the above examples. This can be ascribed to the reduced side reactions between $LiFePO_4$ and electrolyte by the carbon coating layer which prevents $LiFePO_4$ particles from directly contacting with electrolyte. It has been reported that $LiFePO_4$ electrodes tend to release iron ions into the electrolyte when aged at high temperature, thus a significant capacity fade was found when cycled at 37 °C and 55 °C.[23] The dissolved Fe^{2+} can migrate to the negative electrode and deposit on the surface of the graphite anode, leading to a significantly increased interfacial impedance of the graphite electrode due to the possible catalytic effects of the metallic iron particles.[23] Therefore, suppressing the dissolution of Fe from the olivine is very important for the improvement of cycling performance of the olivine/graphite system. $LiFePO_4$ with a more full carbon coating would better retard Fe ion dissolution, as has been demonstrated by the investigation of S. W. Oh *et al.* on a carbon single-coated $LiFePO_4$ and a carbon double-coated $LiFePO_4$.[24] They found that the amount of dissolved Fe after storage in 20 cc of 1 M $LiPF_6$ electrolyte for one week at 60 °C decreased from 55 ppm in the former case to 33 ppm in the latter case. Compared to the single-coated sample, the double-coated $LiFePO_4$ accounts for a more uniform and full coating layer, and thus can deliver stable cycle response even at 60 °C *versus* the graphite anode.

The full carbon coating layer improves not only the electrochemical cycling stability of $LiFePO_4$ but also the $LiFePO_4$'s chemical stability under air exposure. Fe(II) is quite unstable in atmospheric air where O_2 and moisture co-exist. For example, the first charge capacity of the $LiFePO_4$ with air exposure was found to be lower than the first discharge capacity because some surface Fe(II) had been oxidized into Fe(III).[25] The nanosizing of $LiFePO_4$ would aggravate such instability due to the much increased exposure area, leading to a poor storage life of $LiFePO_4$ material. As reported, the nanosized (*ca.* 40 nm) $LiFePO_4$ without carbon full coating was obviously oxidized after only one day's exposure to air at room temperature.[26] With full carbon coating, the nanosized $LiFePO_4$ (20–40 nm) after a long term air exposure (two months) can still deliver a capacity of 170 mA h g^{-1} at the first charge process and a capacity of 160 mA h g^{-1} at the first discharge process, similar to those of the fresh-prepared $LiFePO_4$/C sample, indicating high stability of this full carbon coated $LiFePO_4$ at room temperature storage.[27]

Apart from $LiFePO_4$, attention is also paid to the other lithium metal phosphates. The redox potential of Mn^{3+}/Mn^{2+}, Co^{3+}/Co^{2+}, and Ni^{3+}/Ni^{2+} in the phosphates is tuned to 4.1, 4.8, and 5.1 V, respectively.[28] The high upper charge voltages of $LiCoPO_4$ and $LiNiPO_4$ mean that significant advances in electrolyte chemistry must be made before they can be put to use. In comparison, $LiMnPO_4$ has a compatible potential to commercial 4 V class cathodes, well within the anodic stability limits of aluminium current collectors and alkyl carbonates (*e.g.* propylene carbonate, ethylene carbonate, and diethyl carbonate)/$LiPF_6$ electrolytes. Besides, $LiMnPO_4$ is also attractive due to its higher energy density (1.2 times more) than that of $LiFePO_4$. However, the electrochemical activity of $LiMnPO_4$ is very poor due to the low ionic and electronic conductivity from the heavy polaronic holes localized on the Mn^{3+} sites (the Jahn-Teller ion), and the interface strain between the $LiMnPO_4$ and $MnPO_4$ phase.[29] The electronic conductivity of $LiMnPO_4$ is even lower, *e.g.* $<10^{-10}$ S cm^{-1}, compared with 1.8×10^{-8} S cm^{-1} for $LiFePO_4$.[30] So, the key to the utilization of the $LiMnPO_4$ as practical electrode would be the design of suitable synthesis methods to achieve $LiMnPO_4$ with carbon coating.

I. Taniguchi *et al.* prepared pure $LiMnPO_4$ particles by an ultrasonic spray pyrolysis method, then coated the $LiMnPO_4$ with acetylene black in a weight ratio of $LiMnPO_4 : C = 80:20$ through a dry ball-milling process followed by heat treatment for 4 h in a $N_2 + 3\%H_2$ atmosphere. The obtained C–$LiMnPO_4$ composite can exhibit a discharge capacity of 70 mA h g^{-1} at room temperature and 140 mA h g^{-1} at 55 °C with a charge/discharge rate of C/20.[31] Using a similar procedure, spray pyrolysis followed by ball milling, S. M. Oh *et al.* also obtained carbon-coated $LiMnPO_4$ nanocomposites and investigated the effect of the carbon content (from 10% to 40%) on the physicochemical and electrochemical properties of this material. They found that 30 wt% acetylene black (AB) in the C–$LiMnPO_4$ composite exhibited the best electrochemical performance (Fig. 6), delivering discharge capacities of 158 mA h g^{-1} and 107 mA h g^{-1} at rates of 1/20C and 2C, respectively, which are the highest capacities reported so far for a $LiMnPO_4$ electrode.[32] And the capacity retention of the composite electrode with 30 wt% AB content after 50 cycles was 94.2% at 25 °C and 87.7% at 55 °C, with its initial capacity at 0.5C rate being 137 mA h g^{-1} and 166 mA h g^{-1}, respectively. The results were ascribed to the homogeneous coating of the AB carbon at 30 wt%, which protected the C–$LiMnPO_4$ against HF attack, leading to a significant

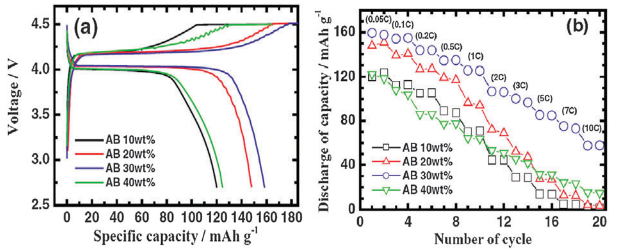

Fig. 6 First charge/discharge curves (a) and rate capability (b) of Li/C–$LiMnPO_4$ cells with different amounts of acetylene black. The cells were charged at a constant current rate of C/20 to 4.5 V, held at 4.5 V until C/100, and discharged at a constant rate of C/20 to 2.7 V. Ref. 32, Copyright 2010, Wiley-VCH.

reduction in Mn dissolution, a lower charge-transfer resistance, and a greatly enhanced electronic conductivity. Besides $LiMnPO_4$, a replacement of 20% Mn by Fe in $LiMnPO_4$, thus forming a $LiMn_{0.8}Fe_{0.2}PO_4$ compound, also demonstrated the properties of a highly interesting and important cathode material, as reported by S. K. Martha *et al.*[33] They prepared carbon-coated $LiMn_{0.8}Fe_{0.2}PO_4$ with 10% carbon content by solid-state synthesis of high energy ball milling. TEM shows that the obtained $LiMn_{0.8}Fe_{0.2}PO_4$ particles are 25–60 nm in diameter and covered by a 5 nm thick carbon film (Fig. 7a, b). When charged/discharged at 1/20 C, this material delivers a capacity of 165 mA h g^{-1}, close to the theoretical one. This compound is in fact a true solid solution of $LiMnPO_4$ and $LiFePO_4$, as demonstrated by its voltage profile, which nicely reflects the redox reaction of both Mn^{2+}/Mn^{3+} and Fe^{2+}/Fe^{3+} with the expected proportional contributions (Fig. 7c). The measurements of this carbon-coated $LiMn_{0.8}Fe_{0.2}PO_4$ nanocomposite after prolonged aging in standard solutions at elevated temperatures and after cycled charge/discharge clearly indicated that its surface stability was much greater than that of Li_xMO_y compounds. The carbon coating enables the active mass to have excellent electronic conductivity and also serves as a barrier against detrimental surface reactions between the active mass and solution species, thus the Li/$LiMn_{0.8}Fe_{0.2}PO_4$ cell showed very high stability and excellent rate capability (Fig. 7d). The observed excellent electrochemical performance of C–$LiMn_{0.8}Fe_{0.2}PO_4$ made it a practically important novel cathode material for safe and long-lived lithium batteries with high power and high energy density.

3.2 $LiMO_2$

Layer structured lithium metal oxides ($LiMO_2$, M = Co, Ni, Mn) with rhombohedral α-$NaFeO_2$ crystal structure have been proven particularly well-suited for application as cathode materials in secondary lithium batteries. $LiCoO_2$ is the most widely used cathode material in commercial lithium-ion batteries, however, its toxicity, safety problems, and high cost of cobalt are still issues of great concern, and suitable alternatives have always been pursued. $LiNi_{0.5}Mn_{0.5}O_2$ has, in comparison with $LiCoO_2$, a high thermal stability in addition to being a relatively low-cost material, and thus is extensively studied as one promising alternative cathode material. In $LiNi_{0.5}Mn_{0.5}O_2$, the average oxidation state of Mn is tetravalent, so that the electrochemically inactive tetravalent Mn provides significant structural stability and results in a simple topotactic reaction maintaining the hexagonal phase during electrochemical cycling, even at the high voltage.[34] However, with the high-power consuming electric devices, modification of $LiNi_{0.5}Mn_{0.5}O_2$ is needed to further improve its performance during cycling at a high rate. J. B. Goodenough *et al.* investigated the influence of carbon coating on the performance of a $LiMn_{0.5}Ni_{0.5}O_2$ cathode by using resorcinol-formaldehyde (R-F) polymer as the carbon source.[35] They found that the carbon coating increased the discharge capacities at relatively high current densities and reduced the capacity fade of $LiMn_{0.5}Ni_{0.5}O_2$ cells by increasing the electronic conductivity between particles and preventing oxygen evolution during charging. Surface modification of

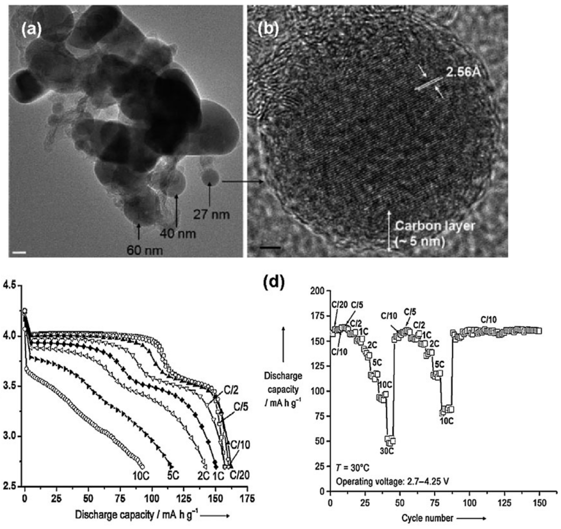

Fig. 7 HRTEM images (a, b) of C–$LiMn_{0.8}Fe_{0.2}PO_4$ particles, the scale bars of (a) and (b) are 20 nm and 2 nm, respectively; (c) typical voltage profiles and (d) cycling behavior of Li/C–$LiMn_{0.8}Fe_{0.2}PO_4$ cells measured at various discharge rates at 30 °C in the standard electrolyte solution. Ref. 33, Copyright 2009, Wiley-VCH.

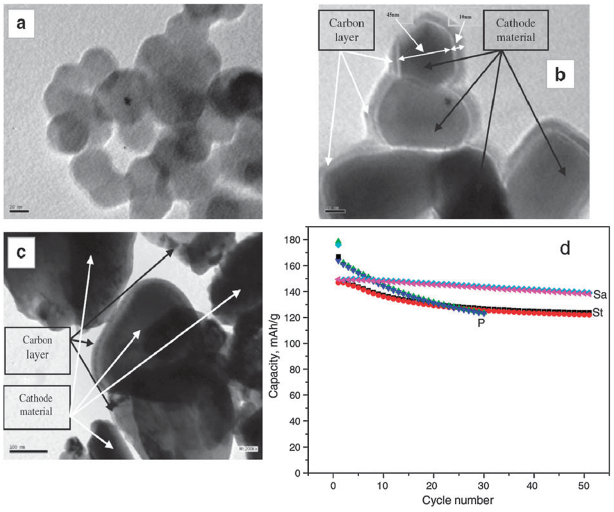

Fig. 8 TEM observations of $LiNi_{0.5}Mn_{0.5}O_2$, (a) bare sample (P), (b) sample coated with sucrose (Sa), (c) sample coated with starch (St); and (d) cycle performances of the three samples. The scale bars of (a), (b) and (c) are 20 nm, 20 nm, and 100 nm, respectively. Ref. 34, Copyright 2010, Springer Link.

$LiNi_{0.5}Mn_{0.5}O_2$ by carbon can also be achieved by calcination of the mixture of $LiNi_{0.5}Mn_{0.5}O_2$ and sucrose (or starch) at 600 °C for half an hour in air.[34] The obtained samples showed clearly the presence of a thin carbon layer (10–12 nm) surrounding $LiNi_{0.5}Mn_{0.5}O_2$ particles (Fig. 8). About 92% and 82% capacity retention was obtained at the 50th cycle for coated $LiNi_{0.5}Mn_{0.5}O_2$ using sucrose and starch, respectively; whereas, 75% was retained after only the 30th cycle for carbon free $LiNi_{0.5}Mn_{0.5}O_2$ (Fig. 8d). The thin carbon layer functions as a protective layer to cover the active sites in the nanoparticles and reduce the electrolyte decomposition, thus improving the electrochemical performance of $LiNi_{0.5}Mn_{0.5}O_2$.

Another alternative to address the challenges of $LiCoO_2$ is to substitute Co by other metals (Ni or Mn) to form layer structured $LiMO_2$ solid solutions that are cheaper, less toxic, safer, and can store more charge (lithium) on charge/discharge cycling. $LiNi_{1/3}Co_{1/3}Mn_{1/3}O_2$ can exhibit reversible capacities of $\sim$200 mA h g^{-1} between 2.8 and 4.6 V, and $\sim$160 mA h g^{-1} between 2.5 and 4.4 V, much larger than that of $LiCoO_2$, and thus has been considered as a candidate to replace commercial $LiCoO_2$. However, its electronic conductivity is relatively lower than that of $LiCoO_2$. Since the preparation of $LiNi_{1/3}Co_{1/3}Mn_{1/3}O_2$ needs air atmosphere, it is difficult to apply carbon coating through the conventional pyrolysis of organic compounds in inert atmosphere at high temperature (700–900 °C). However, attempts have been made by either using carbon sources with low pyrolysis temperature, such as table sugar,[36] polyvinyl alcohol[37] and a low heat treatment temperature (300 °C for 3 h),[38] or a quite short heating time (600 °C for 0.5 h in air),[39] or a special coating technique such as microwave plasma chemical vapor deposition.[40] Positive gains obtained by these attempts include: improved thermal stability,[36,38] decreased charge transfer resistance,[37] enhanced rate capability[38,40] and cycle performance.[39,40]

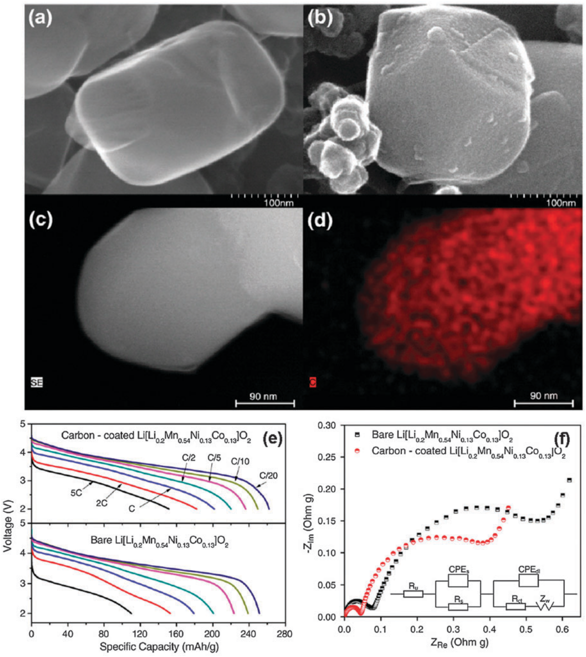

Fig. 9 (a) SEM images of the bare (a) and carbon-coated (b) $Li[Li_{0.2}Mn_{0.54}Ni_{0.13}Co_{0.13}]O_2$ particles, (c) STEM image and (d) carbon map of the carbon-coated $Li[Li_{0.2}Mn_{0.54}Ni_{0.13}Co_{0.13}]O_2$ particle, (e) discharge profiles at various rates and (f) EIS plots of the bare and carbon-coated $Li[Li_{0.2}Mn_{0.54}Ni_{0.13}Co_{0.13}]O_2$ electrodes. Ref. 43, Copyright 2010, Elsevier.

Recently, solid solutions between $Li[Li_{1/3}Mn_{2/3}]O_2$ and $LiMO_2$ (M = Mn, Co, and Ni) have become more and more appealing due to their much higher capacities of $\sim$250 mA h g^{-1} and lower cost and better safety compared to $LiCoO_2$. However, the low rate capability arising from the low electronic conductivity induced by the insulating $Li[Li_{1/3}Mn_{2/3}]O_2$ component[41] and the thick solid–electrolyte interfacial (SEI) layer formed at operating voltages as high as 4.8 V[42] remain big challenges for the application of these cathodes in EV and HEV. Modification of the surface with conductive agents turns out to be a feasible approach to suppress the SEI layer thickness and enhance the surface conductivity. J. Liu *et al.* successfully applied carbon coatings on the layered $Li[Li_{0.2}Mn_{0.54}Ni_{0.13}Co_{0.13}]O_2$ cathode by thermal evaporation of a high purity graphite rod inside a JEOL thermal evaporator under high vacuum of $\sim 10^{-7}$ Torr.[43] The carbon mapping image confirmed a carbon coating layer on the material surface, as shown in Fig. 9. Surface electronic conductivities of the bare and the carbon coated $Li[Li_{0.2}Mn_{0.54}Ni_{0.13}Co_{0.13}]O_2$ electrodes were found to be 0.696 and 0.975 S cm^{-1}, respectively, indicating a 40% enhancement by coating with carbon. The carbon-coated $Li[Li_{0.2}Mn_{0.54}Ni_{0.13}Co_{0.13}]O_2$ electrodes exhibited much better rate capability compared to the bare sample (Fig. 9e). EIS measurements revealed that the improved electrochemical performance of the carbon-coated sample was due to the enhancement in surface electronic conductivity and the suppression of SEI layer development, as shown in Fig. 9f.

4. Carbon coatings for anode materials

4.1 $Li_4Ti_5O_{12}$

Spinel $Li_4Ti_5O_{12}$ is a very promising anode material with high safety due to the absence of SEI film: its flat discharge platform at about 1.55 V *versus* Li/Li^+ is above the reduction potential of most electrolyte solvents so as not to reduce the solvent and form a solid electrolyte interface, furthermore, the voltage is sufficiently high to remove the possibility for lithium plating. $Li_4Ti_5O_{12}$ has high reversible capacity (175 mA h g^{-1}) and extremely small structural change during lithium insertion/extraction (zero-strain), which ensures a good reversibility and structural stability in a long cycling life.

For security and cycling stability concerns, $Li_4Ti_5O_{12}$ is highly promising for large-scale long-life energy storage batteries. However, $Li_4Ti_5O_{12}$ has pretty low electronic conductivity (*ca.* 10^{-13} S cm^{-1}) and Li^+ diffusion coefficient (10^{-9}–10^{-13} cm^2 s^{-1}); thus the high rate performance is not satisfied for such applications.[44,45] Two typical approaches have been developed over the past few years to resolve this problem. One is to develop the nanoparticles, which can reduce the Li-ion diffusion path as well as provide large contact area between the electrode and electrolyte.[46–49] The other is to improve the electrical conductivity by coating conductive materials on the $Li_4Ti_5O_{12}$ surface.[50–54] For example, a porous microspherical $Li_4Ti_5O_{12}$ coated with 7.0 wt% N-doped carbon can deliver a reversible capacity of 161 mA h g^{-1}, 145 mA h g^{-1} and 129 mA h g^{-1} at a current rate of 0.5C, 5C and 10C, respectively; while the uncoated sample only delivers 60 mA h g^{-1} and 15 mA h g^{-1} at a current rate of 5C and 10C, respectively, which well shows the important role of carbon coating in the performance of $Li_4Ti_5O_{12}$.[50] However, these previous studies about $Li_4Ti_5O_{12}$ generally focused on the "conductive surface modification" and "nano-size" separately, rather than considering both of them together. Challenges are that high crystallinity is required for $Li_4Ti_5O_{12}$ to get good electrochemical performances. However, the main approach for the preparation of nanostructured $Li_4Ti_5O_{12}$ can only afford a low annealing temperature or a quite short annealing period in order to prevent the product from aggregating. The difficulty is that: most titanium salts (the starting precursors) are easily hydrolyzed to TiO_2; once TiO_2 is formed, it is necessary to heat it with lithium salts (Li_2CO_3 or LiOH *etc.*) at high temperature (750 °C or above) for a long time to obtain well-crystallized $Li_4Ti_5O_{12}$, which leads to a much increased particle size of the final product.

Recently, our group developed a facile method to prepare carbon-coated $Li_4Ti_5O_{12}$ nanoparticles, in which both "nanosize" and "double surface conductive modification based on Ti(III) and carbon" can be achieved simultaneously.[55] In this method, nanosized TiO_2 with polyaniline (PANI) coatings was first synthesized through the concurrence of hydrolysis of $Ti(OC_3H_7)_4$ and polymerization of aniline, then the PANI-coated TiO_2 was coupled with a lithium salt and calcined at 800 °C for 24 h to form crystalline $Li_4Ti_5O_{12}$ and at the same time carbonize the PANI. The carbonization of PANI can effectively restrict the particle-size growth of $Li_4Ti_5O_{12}$, thus the obtained $Li_4Ti_5O_{12}$ can remain small, of a size of 50–70 nm, even after such a long-time and high-temperature heat treatment, as shown in Fig. 10. In addition, the carbonization of PANI also reduced some of the surface Ti(IV) to Ti(III). The Ti(III) surface modification can not only enhance the surface electronic conductivity, but also increase the single-phase insertion/extraction ($Li_{4+\delta}Ti_5O_{12}$ or $Li_{7-\gamma}Ti_5O_{12}$) region outside the two-phase region. Such carbon–Ti(III) double surface modification combined with tailored particles size promised synergic beneficial effects, such as high surface conductivity, shortened Li-ion diffusion paths and increased equilibrium solid solution region, thus the prepared $Li_4Ti_5O_{12}$ demonstrated a high rate performance, *e.g.* 160 mA h g^{-1} at a current density of 0.1 A g^{-1} and 70 mA h g^{-1} even at 3.0 A g^{-1} (Fig. 10d).

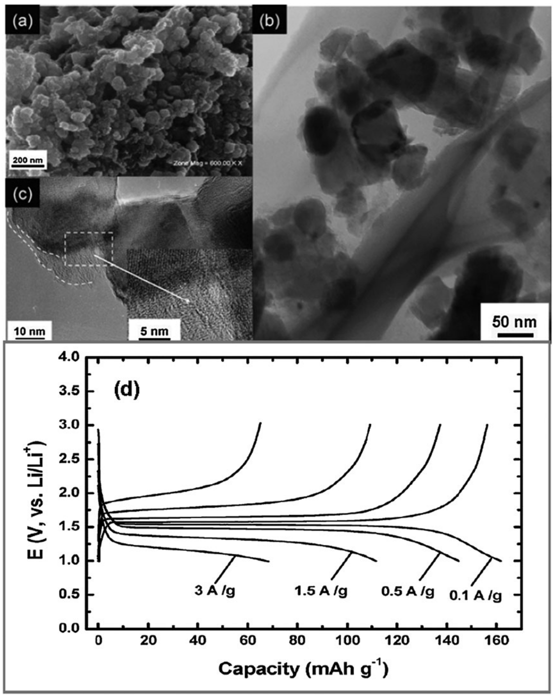

Fig. 10 SEM image (a), TEM images (b, c), and charge/discharge tests at different current densities (d) of carbon–Ti(III) double surface modified $Li_4Ti_5O_{12}$ material. Ref. 55, Copyright 2009, The Royal Society of Chemistry.

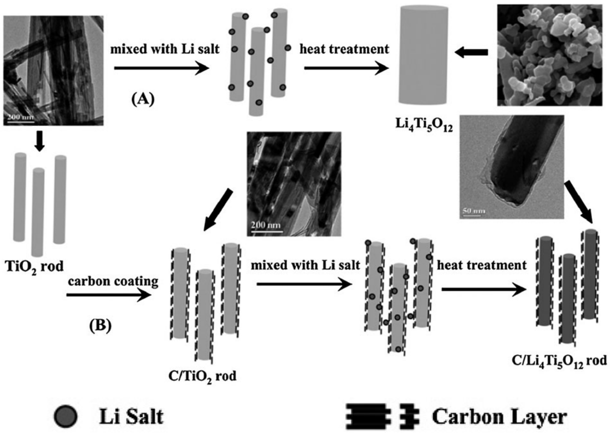

Fig. 11 Schematic presentation of the conventional solid-state process (A) and carbon pre-coating process (B) to prepare $Li_4Ti_5O_{12}$ from the TiO_2 precursor. Ref. 56, Copyright 2010, The Royal Society of Chemistry.

The above strategy to prepare carbon-coated $Li_4Ti_5O_{12}$ nanocomposites involved a novel role of the carbon coating layer: the dimension restrictor. This role shows a great effect in the synthesis of nanostructures. L. Cheng *et al.* successfully prepared carbon-coated $Li_4Ti_5O_{12}$ of various morphologies, *e.g.* nanorods, hollow spheres and nanoparticles, *via* a simple carbon pre-coating process in which the nanostructured TiO_2 was first coated with a carbon layer by chemical vapor deposition (CVD), followed by a solid-state reaction with lithium salt.[56] The coated carbon layer well prevented the particles from aggregating and thus enabled the produced $Li_4Ti_5O_{12}$ to maintain a similar structure as that of its TiO_2 precursor. Fig. 11 gives the comparison of morphology changes between the conventional solid-state process and pre-coating process by using nanorods as the example.[56] Similar results were also obtained in terms of hollow spheres and nanoparticles. In all cases, the process without pre-coating of carbon layer would lead to the total loss of the nanomorphology. While the process with pre-coating of carbon layer well kept the morphology of the TiO_2 precursor, showing the important role of a carbon layer as the dimension restrictor during high temperature annealing.

4.2 Graphite

It is generally accepted by the battery community that graphite electrodes will remain the most important and relevant anodes in Li-ion batteries for a long time due to their advantages such as a flat and low voltage range, high reversible capacity (372 mA h g^{-1} with the stoichiometry of LiC_6), and low cost. Li graphite electrodes are naturally passivated in alkyl carbonate solutions, the passivating solid electrolyte interface (SEI) can prevent further decomposition of the electrolyte in the following cycles and prohibit the solvent molecules passing through to intercalate into the graphite host, and thus is essential for the stability of a graphite electrode.[3] The formation of this SEI film strongly depends on the surface structure of graphite and the type of the used electrolyte. There are two kinds of planes on graphite crystallite surface, edge and basal. The exfoliation of graphite and decomposition of the electrolyte mainly occur on edge planes rather than on basal planes. In addition, surface functional groups are also responsible for the instability of graphite during the charge/discharge process.[6] As for the electrolyte type, propylene carbonate (PC)-based electrolytes are known not to result in the efficient passivating SEI film.[3] While in ethylene carbonate (EC)-based electrolyte, the graphite electrodes are well-passivated and intercalate Li ions reversibly. Unfortunately, EC has a much higher melting point than PC (mp_{EC} 39 °C; mp_{PC} −49 °C), which will limit its utilization at low temperatures.[57]

Research on the graphite anode mainly focuses on reducing the irreversible capacity (increasing the coulombic efficiency) associated with the first charge cycle which limits the performance of the cells. The irreversible capacity arises from the formation of SEI and other side reactions such as decomposition of the electrolyte, exfoliation of the graphite and reduction of the functional groups on the graphite surface. Carbon coating has been proved to be an effective approach to improve the electrochemical performances of graphite. Thermal or chemical vapor decomposition (TVD or CVD) has been the most widely used method to coat carbon onto the graphite surface.[58–60] This method promises homogeneous deposition of the carbon layer on the surface of the core material, which in turn forms a core–shell-structured composite with a uniform thin carbon coating, as shown in Fig. 12.[58] After coating, the surface properties of the graphite electrode changed, *e.g.*, the disorder and O/C ratio on the surface decreased as evidenced by Raman spectroscopy and ESCA analysis. It is probable that the SEI film formed on the pristine graphite contains lots of pores, through which electrolyte decomposition by LiC_6 takes place, resulting in a thicker SEI layer and thus lower coulombic efficiency. Comparatively, the SEI layer formed on the coated graphite is more compact and thin, and thus results in high coulombic efficiency (Fig. 12).[58] Direct observation of such difference in the SEI film has been obtained by H. L. Zhang *et al.*: the SEI film for pyrolytic carbon coated natural graphite spheres was found to be more compact, and its thickness was about 60–150 nm, much thinner than that (450–980 nm) on the surface of original natural graphite spheres.[59]

M. Yoshio *et al.* applied carbon coating by a TVD method and systematically investigated the effect of carbon coating on the electrochemical performances of natural graphite.[57,61–64] The coated natural graphite showed much improved electrochemical performances including larger reversible capacity, better cycling behavior and higher coulombic efficiency in the first cycle in both PC-based and EC based electrolytes than the bare natural graphite. They found that the weight portion of carbon coating in the composite material played an important

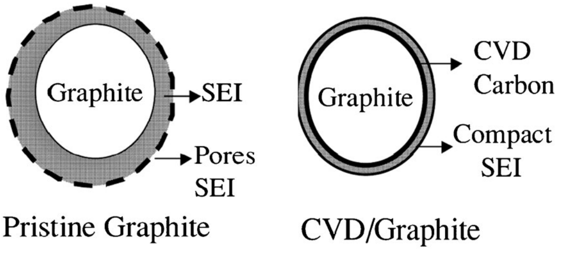

Fig. 12 Simple model to show the SEI on pristine and CVD carbon coated graphite sample. Ref. 58, Copyright 2001, Elsevier.

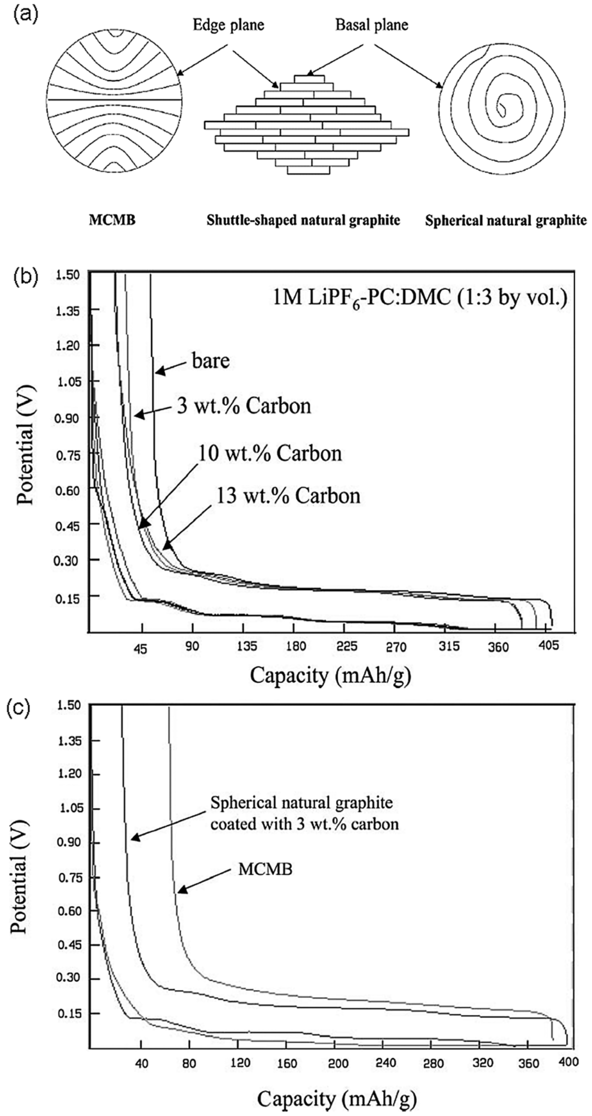

Fig. 13 (a) Schematic views of the MCMB, shuttle-shaped and spherical natural graphite, (b) initial charge/discharge curves for the spherical natural graphite coated with different amounts of carbon, (c) initial charge/discharge curves of MCMB and spherical natural graphite coated with 3 wt% carbon, in the electrolyte of 1 M $LiPF_6$ dissolved in the mixture solvents of PC and DMC (1 : 3 by volume). Ref. 57, Copyright 2004, The Royal Society of Chemistry.

role in controlling the electrochemical characteristics.[61,62] The inertness of the carbon-coated graphite to the electrolytes increased with an increase in the amount of carbon coating. However, the electrode density would decrease with the increase of the carbon coating amount. Too much carbon coating would also decrease the discharge capacity of the composite electrode. To maintain the inertness and at the same time decrease the carbon coating amount, they modified the morphology of natural graphite from originally anisotropic flaky to spherical shapes by sphere-making process, and then coated carbon on the spherical graphite.[57,64] The spherical graphite samples demonstrated much higher coulombic efficiency values than the corresponding shuttle-shaped graphite sample with similar amounts of carbon coating.[64] Compared to the shuttle-shaped graphite, the spherical graphite greatly reduced the exposure of surface edge planes towards electrolyte, as shown in Fig. 13a, and thus a very low amount of carbon coating was sufficient to cover all the edge planes and active sites on the surface of the graphite core.[57] For example, the influence of only 3 wt% carbon coating on covering the surface of the spherical natural graphite "core" and preventing PC decomposition has been already comparable to the carbon-coating amount of 10 and 13 wt% (Fig. 13b). Besides, the 3 wt% carbon coated spherical natural graphite demonstrated superior advantages over the "traditional" highly graphitized mesocarbon microbeads (MCMB) in many respects such as high rate capacity, high coulombic efficiency, low irreversible capacity, and low cost (Fig. 13c). Moreover, the recent investigation of Y. S. Park *et al.* revealed that the surface modification of coating with a non-graphitic carbon layer on natural graphite can also improve the thermal stability of spherical natural graphite.[65] The surface modification resulted in a drastic decrease in the BET surface area (from 5.67 $m^2\ g^{-1}$ to 0.6 $m^2\ g^{-1}$). DSC studies on the fully-lithiated state of a graphite electrode performed at elevated temperature showed a better stability after carbon-coating. The reason was attributed to that the non-graphitic carbon layer suppressed the release of intercalated lithium from natural graphite at high temperatures, as analyzed by XRD data.

4.3 Alloy anode

A number of metals and semiconductors, *e.g.* Sn, Sb, Ge and Si, react with lithium to form alloys by electrochemical processes that are partially reversible and are of low voltage. They are able to store large amounts of lithium per formula and are thus of great interest as high capacity anode materials, typically as $Li_{4.4}Sn$ (993 mA h g^{-1} and 1000 mA h cm^{-3} *versus* 372 mA h g^{-1} and 855 mA h cm^{-3} for graphite) and $Li_{4.4}Si$ (4200 mA h g^{-1} and 1750 mA h cm^{-3}). Unfortunately, the accommodation of so much lithium is accompanied by enormous volume changes in the host metal plus phase transitions, *e.g.* a volume change over 300% for pure Sn and Si in their full lithiated state ($x = 4.4$). The mechanical strain generated during the alloying/de-alloying processes leads to rapid deterioration of the electrode: cracks and, eventually, pulverization. As a result, the contact between the active material and the current collector becomes loose, and these alloys present very poor cyclic characteristics. Significant research efforts have been devoted to overcome this problem, which leads to the conclusion that any physical or chemical means of buffering the reactant expansion, maintaining the electrode integration and electrical contacts between particles should be beneficial.

Early investigation done by M. Yoshio *et al.* obtained improved electrochemical performances by coating carbon onto the surface of microsized Si particles (10 μm) using a thermal vapor decomposition technique.[66] The carbon-coated Si with a carbon content of ~10 wt% showed high reversible capacity over 800 mA h g^{-1}, high coulombic efficiency, satisfactory compatibility with both the EC and PC-based electrolytes, and better thermal stability than that of graphite. The carbon-coating on the outer layer of Si was thought to suppress the high decomposition of electrolyte on the surface of Si-based electrodes, help to provide electric contact networks around Si particles, thus to maintain high capacity during 20 cycles of charge/discharge.[67] However, this is still not enough to have long term cycling performance since the electric network established by solely a thin layer of surface carbon coating is easy to break due to the large volume change within the microsized alloy particles.

One of the effective strategies is to prepare intermetallic compounds (M′M), which consist of an inactive phase M′ that does not react with lithium and an active phase M that reacts with lithium, such as Cu–Sn, In–Sb, Co–Sn, Sn–Fe, *etc.* The introduction of inactive phase M′ can reduce the volume of expansion/contraction to a considerable extent, thus, improving the cycling performance compared to pure Sn at the price of decreased specific capacity. However, these intermetallic compounds are typically prepared by high-temperature annealing, mechanical alloying or melt-spinning, in which the particle size is generally in micrometres. Such large particles still suffer pulverization during long term cycling. Another effective strategy is fabricating fine active nanoparticles dispersed/encapsulated within a solid, mixed conducting matrix, *e.g.* Sn-nanocrystallite in mesoporous carbon,[68] SnO_2-nanocrystal in graphene sheets,[69] SnO_2-nanoparticle in amorphous carbon,[70] Si-nanocrystallite in carbon aerogel.[71] The presence of large amounts of well-distributed carbon material in these nanocomposites can maintain an integral and continuous electric conductive network upon repeated charge/discharge, thus leading to substantial improvements in cyclability. For example, Sn-nanocrystallite encapsulated in mesoporous carbon (contains ~21% carbon) maintained a nearly constant capacity of above 710 mA h g^{-1} for up to 50 cycles; while the pure Sn nanoparticles (~100 nm) lost all of their initial capacity after 25 cycles (from 1018 mA h g^{-1} to 0 mA h g^{-1}).[68] Si nanocrystalline/amorphous carbon nanocomposites (contain ~56% carbon) can maintain 43% of their initial reversible capacity during 100 cycles, while pure nanocrystalline Si (<100 nm) only retained 0.3% of its capacity after 100 cycles.[72] However, these nanocomposites usually contain a high carbon content (30–50% in weight), which leads to a decreased overall electrode capacity.

Recently, carbon coated nanosized Si or Sn-based materials with core–shell structures have attracted more attention due to their superiority in both cyclability and rate performance.[73–77] The carbon shell prevents the aggregation and pulverization of the nanosized core particles, and allows for a very good interparticle electrical contact, which enables us to extract

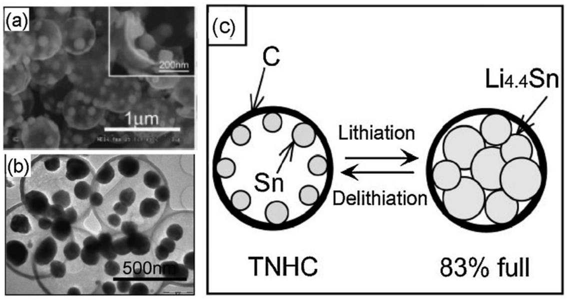

Fig. 14 SEM (a) and TEM (b) of tin nanoparticles encapsulated in hollow carbon spheres (TNHC); (c) schematic illustration shows how such a hollow core–shell structure buffers the volume expansion during Li^+ insertion/retraction. Ref. 14, Copyright 2008, Wiley-VCH.

the high capacity of the active core nanoparticles, at relatively high rates; the thin carbon shell also has some elasticity to accommodate the strain of volume change during Li^+ insertion/extraction, improving the reversibility and electrode integration. For example, the carbon coated $Si_{70}Sn_{30}$ nanoalloys with a particle size <10 nm and a carbon content of ~10 wt% can deliver a reversible capacity of 2032 mA h g^{-1} at 0.2C and a high capacity retention of 97% after 60 cycles,[73] the good performance results from both a small particle size and the tightly packed carbon coating layer. The core–shell carbon coated Cu_6Sn_5 (with a particle size of 20–30 nm and a carbon content of ~23 wt%) showed nearly no capacity fading during 50 cycles of charge/discharge, in comparison, the uncoated nanosized Cu_6Sn_5 (also 20–30 nm) obtained by a similar synthesis procedure lost 64% of its capacity after 50 cycles.[75] Besides, hollow core–shell structures, which can provide additional void to buffer the volume expansion in spite of the elastic carbon shell, are further developed to promote the electrochemical properties of alloy-based materials.[14,78–80] For example, the tin nanoparticles encapsulated in hollow carbon spheres (Fig. 14) showed an extended cycle life to 100 cycles;[14] the SnO_2/carbon hollow nanospheres demonstrated a reversible capacity of 473 mA h g^{-1} after 50 cycles, while the capacity of pure SnO_2 hollow spheres decreased to below 300 mA h g^{-1} after 40 cycles.[78]

5. Challenges and perspectives

5.1 Applicable methods for specific active material

Up to now, various carbon coating technologies have been developed for different electrode materials, as summarized in Table 2. Since the synthesis of $LiMPO_4$ and $Li_4Ti_5O_{12}$ usually involves high temperature annealing in inert atmosphere, it is convenient to introduce carbon sources during the synthesis procedure and realize carbon coating with high conductivity due to the high temperature treatment. On the other hand, they are both very poor electronic conductors, and thus carbon coating plays an especially vital role in their electrochemical performances. As can be seen from the examples in Table 2, nearly all the developed methods, such as sol–gel, spray pyrolysis, ball-milling, co-precipitation, CVD *etc.* can be used for coating carbon on $LiMPO_4$ and $Li_4Ti_5O_{12}$. Among them, the strategies which involve first pre-coating of $M_x(PO_4)_y$ or TiO_2 by carbon precursors and then combination with Li salt to produce $LiMPO_4$ or $Li_4Ti_5O_{12}$ show the highest superiority in electrochemical behavior due to the fact that they favor a more uniform full coating and synergy effect with nanosize. Now, "nanosize" together with "carbon coating" has been considered as the most promising way to obtain both large capacity and high rate performance, and is attracting more and more research efforts in the synthesis of $LiMPO_4$ and $Li_4Ti_5O_{12}$ based materials.

For graphite, which has already a high conductivity, the main purpose of carbon coating is to reduce the surface activity towards side reaction and modify the formation of SEI film. The most frequently used method is chemical/thermal vapor deposition technology. By selecting different carbon sources and controlling the deposition time and temperature, the carbon content and coating thickness can be adjusted. To realize scale production, a special reactor such as a fluidized bed reactor has been designed for the CVD coating of graphite.

As for alloy-type anodes, it is difficult to assure the integration and conductivity contact of the electrode by solely a thin layer of carbon coating on the surface of an alloy, since the alloy experiences enormous volume changes during cycling that a fresh surface of active material is continuously generated for every cycle. With the development of nanotechnology, alloy anodes with unique morphologies such as core/shell and hollow structures demonstrated superior electrode performances with much longer cycle stability as well as improved rate capability. However, these nanostructures require a special design of the synthesis strategy and very complex synthetic techniques, as listed in Table 2. These multi-step synthesis routes are of high cost and are difficult to realize scale production. Rather than surface carbon coating, the more preferred way for alloy type anodes is to disperse the alloy nanoparticles in a carbon matrix, which in fact refers to an alloy/carbon composite with a quite high carbon content, as done in ref. 68–72. To get ultrafine alloy nanoparticles, the solution-based methods are mainly used, which typically involve the *in situ* reduction from a metal salt to an alloy in the presence of carbon sources. Other methods such as high energy ball-milling can also produce highly distributed alloy particles in a conductive matrix. Any way, these composites with an alloy embedded in carbon might be a promising direction for future development of alloy type anodes in our point of view.

Although carbon coating has demonstrated impressive advantages in performance promotion for many electrode materials, it still faces a big bottle-neck for application in lithium transition metal oxide cathodes. Most of the lithium transition metal oxide cathodes are synthesized in air or pure oxygen at temperatures >800 °C. Under such conditions, carbon formed from any added organic precursors either during synthesis or in a post-treatment step is likely to burn out, leading to nearly no residue of the carbon component. As shown in Table 2, the residue carbon content was no more than 3%. If the calcination is carried out under an inert atmosphere to prevent loss of carbon, the thermal decomposition of carbon sources would generate a strong reductive environment like H_2, CO, or a combination of both, which can easily reduce the transition metal in the oxides and change the valence state of the elements and even the crystal structure of the

Table 2 Different coating methods with their synthetic details and resulting coating features used for the typical cathode and anode materials

Active material	Coating method	Carbon sources	Synthesis procedure	Calcination condition	Structures/particle size carbon content/thickness	Ref.
$LiFePO_4$	Dry mixing	Glucose	$FePO_4$ nanoparticles, Li_2CO_3 and glucose were mixed and ground, then calcined at different temperatures for 12 h	600–800 °C, 12 h in pure N_2	Non-uniform coating, 0.2–2 μm, 2.91–3.37%, NA	17
	Sol–gel	Pyromellitic acid	$LiFePO_4$ precursor was synthesized by a sol–gel method, then the carbon precursor was added with or without catalyst by ball-milling, finally fired at 600 °C	600 °C, 10 h in pure N_2	Non-uniform coating, 0.1–2 μm, 0.3–1.56%, NA	18
	Ball-milling	Polystyrene and malonic acid	$LiFePO_4$ was first prepared by solid-state reaction, then mixed with carbon sources by ball-milling, finally annealed at 600 °C	600 °C, 12 h in Ar + 5%H_2	Non-uniform coating, NA, 1.25–2.54%, 2.0–25 nm	20
	In situ polymerization	Aniline and sucrose	Aniline was *in situ* polymerized on the surface of fresh $FePO_4$ precipitation, then Li salt and sucrose were mixed with $FePO_4$, finally calcined	700 °C, 15 h in Ar + 5%H_2	Core–shell, 20–40 nm, 6%, 1–2 nm	21
	Solution mixing and spray pyrolysis	Graphene oxide	Suspension of nanosized $LiFePO_4$ by hydrothermal reaction was mixed with graphene oxide suspension, then spray dried at 200 °C, finally calcined at 600 °C	600 °C, 5 h in Ar	Nanoparticles wrapped loosely with graphene network, 100 nm[a], 5%, 2 nm	22
	CVD	C_3H_6	$LiFePO_4$ was first prepared by solid-state reaction, then coated with carbon by C_3H_6 gas phase deposition with N_2 flowing at 700 °C	700 °C, 24 h in purified N_2	No details, 300 nm, 3.5%, NA	23
	Co-precipitation plus dry mixing	Sucrose and pitch	$FePO_4$ was prepared by co-precipitation with sucrose, then Li salt and pitch (as second carbon source) was mixed with $FePO_4$ and finally calcined	750 °C, 15 h in Ar + 4%H_2	Double-carbon coating, 200–300 nm[a], 3.1%, NA	24
$LiMnPO_4$	Spray pyrolysis followed by ball-milling	Acetylene black	$LiMnPO_4$ was first prepared by ultrasonic spray pyrolysis, then mixed with acetylene black by dry ball-milling at different conditions, finally heat treated	400–700 °C, 1–4 h in N_2 or Ar	Mixture of $LiMnPO_4$ and carbon particles, NA, 10–40%, NA	31, 32
$LiMn_{0.8}Fe_{0.2}PO_4$	Ball-milling	Carbon	$LiMn_{0.8}Fe_{0.2}PO_4$ was prepared by solid-state reaction, then mixed with carbon by ball-milling, finally calcined	550 °C, 3 h in Ar + H_2	Non-uniform coating, 20–60 nm, 10%, 5 nm	33
$LiNi_{0.5}Mn_{0.5}O_2$	Dry mixing	Sucrose or starch	LNMO was prepared by co-precipitation followed by solid-state reaction, then mixed with carbon sources by grinding, finally heat treated	600 °C, 0.5 h in air	Non-homogenous coating, 40–45 nm, <1%, 10–12 nm	34
$LiNi_{1/3}Mn_{1/3}Co_{1/3}O_2$	Wet mixing	Table sugar	LNMCO by co-precipitation was mixed with sugar for 3 h using ethanol as the solvent, then sintered in air	350 °C, 1 h in air	Non-uniform coating, 2–3 μm, 1–3%, NA	36
	Solution mixing	Polyvinyl alcohol	LNMCO by solid-state reaction was added to the hot water dissolved with a carbon source under stirring, then evaporated the water, finally heat treated	400 °C, 0.5 h in air	Non-uniform and partial coating, 200–700 nm, 0.4–2.0%, NA	37
	Wet mixing	Carbon black	LNMCO by solid-state reaction was mixed with the suspension of dispersed carbon black under stirring, then filtered and dried	300 °C, 3 h in air	Surface covered by carbon particles, 10 μm, 1–3%, NA	38
	Solution mixing	Citric acid	LNMCO particles were dispersed in the ethanol solution of citric acid under stirring and vacuum, then dried and heat treated	600 °C, 0.5 h in air	Surface distributed carbon beads, >2 μm, 0.61%, NA	39
	Microwave-plasma CVD	Anthracene	Microwave Plasma Chemical Vapor Deposition process was carried out at 1200 W microwave radiation power for 2 s	—	Uniform coating, 2 μm, 0.8–1.2%, 10 nm	40
$Li_{1.2}Mn_{0.54}Ni_{0.13}\ Co_{0.13}O_2$	Thermal evaporation	Graphite rod	LMNCO electrode film was first prepared, then coated with carbon by thermal evaporation of graphite inside an evaporator under high vacuum	—	Uniform coating, NA, NA, NA	43
$Li_4Ti_5O_{12}$	Wet mixing	Ionic liquid	Ionic liquid was added to porous $Li_4Ti_5O_{12}$ particles and then the mixture were heated at 600 °C	600 °C in Ar	Thin coating layer of N-doped carbon, NA, 7.0%, NA	50

Table 2 (***continued***)

Active material	Coating method	Carbon sources	Synthesis procedure	Calcination condition	Structures/particle size carbon content/thickness	Ref.
	Sol–gel	Citric acid	Li(Ac)$_2$, Ti(OC$_4$H$_9$)$_4$ and citric acid were dissolved in ethanol and mixed under stirring, the resulted gel was aged, dried and finally calcined	800 °C, 15 h in Ar	Non-uniform coating, 200–700 nm, 2–5.5%, NA	52
	Rheological phase method	PVB	Li$_2$CO$_3$, TiO$_2$ were blended and added into the Polyvinylbutyral(PVB)/ethanol solution, the rheological mixture was stirred, dried and finally calcined	800 °C, 15 h in Ar	Non-uniform coating, 2.1 μm, 0.98%, NA	54
	In situ polymerization	Aniline	Polyaniline coated TiO$_2$ was prepared by hydrolysis of Ti(OC$_3$H$_7$)$_4$ coupled with polymerization of aniline, followed by a solid-state reaction to obtain Li$_4$Ti$_5$O$_{12}$	800 °C, 24 h in Ar + 5%H$_2$	Ti(III) and carbon co-coating, 50–70 nm, 3%, NA	55
	CVD	Toluene	Nanostructured TiO$_2$ was first coated with carbon by a CVD process at 800 °C for 2 h, then followed by a solid-state reaction to obtain Li$_4$Ti$_5$O$_{12}$	800 °C, 9 h in N$_2$	Nanostructures with uniform coating, NA, 3%, 2–5 nm	56
Graphite	CVD	Toluene	Thermal vapor deposition was performed by using N$_2$ as the carrier gas at 950–1000 °C for different seed time of the toluene vapor	950–1000 °C in N$_2$	Uniform coating with controlled weight ratio, NA, 0.3–17.6%, NA	57, 61–64
	CVD	Ethylene	CVD process was performed at 700–1000 °C with 5% ethylene in Ar gas as the source gas for 30–120 min	700–1000 °C in Ar	Uniform coating, NA, 0.2–6%, NA	58
	CVD	C$_2$H$_2$	Thermal decomposition of C$_2$H$_2$ was performed at 950 °C for 10–90 min in a fluidized bed reactor in C$_2$H$_2$/Ar flow	950 °C in Ar	Uniform coating, 20 μm, 13%, 250 nm	59
Si	CVD	Benzene	CVD was performed at 1000 °C in a benzene/N$_2$ flow and repeated for several cycles	1000 °C in N$_2$	Uniform coating, 18 μm, 20%, NA	66
	Spray pyrolysis	Citric acid	Spray pyrolysis of the suspensions consist of Si powder, citric acid and ethanol at 300–500 °C in air	300–500 °C in air	Si in amorphous carbon, 10–100 nm, 27–85%, 1–40 nm	72
Sn	Solution-based synthesis	Glucose	(1) Prepare Sn(IV) acetate nanowires by reflux of tin powder and acetic acid, (2) hydrothermal treatment of the nanowires in the presence of glucose to obtain SnO$_2$/C, (3) reduce SnO$_2$/C to Sn/C by calcination	900 °C, 6 h in Ar + 7%H$_2$	Sn nanocrystallites encapsulated in mesoporous carbon, 5 nm, 21%, NA	68
Si$_{70}$Sn$_{30}$	Solution-based synthesis	Butyllithium	SiCl$_4$ and SnCl$_2$ were reacted with sodium naphthalide using dimethoxyethane as the solvent, then the product was mixed with *n*-C$_4$H$_9$Li, finally concentrated, washed, dried and calcined	900 °C, 5 h in vacuum	Uniform coating, 10 nm, 11%, 2 nm	73
Gu$_6$Sn$_5$	Solution-based synthesis	Resol	(1) Synthesize Cu$_6$Sn$_5$ nanoparticles by sodium borohydride reduction of CuCl$_2$ and SnCl$_4$, (2) treat the particle surface hydrophobic, (3) coat the particles with resol by *in situ* polymerization, (4) calcine the sample to carbonize resol	800 °C, 2 h in N$_2$	Core–shell, 20–30 nm, 23%, 5 nm	75
SnO$_2$	Hydrothermal	Glucose	(1) Synthesize SnO$_2$ hollow spheres by a hydrothermal method, (2) hydrothermal treat the SnO$_2$ spheres in the presence of glucose, (3) carbonize the SnO$_2$/polysaccharide composite hollow spheres	550 °C, 3 h in inert gas	Hollow core–shell, 150–400 nm, 33.5%, NA	78
Sn	Hydrothermal	Glucose	(1) Hollow SnO$_2$ spheres were synthesized by a template method, (2) SnO$_2$/C double shell spheres were obtained by hydrothermal treatment of SnO$_2$ in the presence of glucose, (3) carbonize glucose and reduce SnO$_2$ to Sn by calcination	700 °C, 4 h in N$_2$	Hollow core–shell, 60–100 nm, 26%, 20 nm	14

[a] Denotes the primary particle size.

oxide material.[8] Thus, nearly all the reported examples adopted a post-addition (mechanical mixing) method and a low temperature as well as short annealing time when applying carbon coating. How to develop a relative "cold" technique to realize a carbon-coating layer on the surface of lithium transition metal oxides without a significant negative impact on the substrate material would still be a big challenge faced by the researchers. In this view point, promising ways might be the physical deposition techniques which possibly permit a relative low temperature environment for the substrate material, such as ALD (atomic layer deposition), PLD (pulse laser deposition), magnetron sputtering, and so on.

5.2 Advantages and limits of specific coating technique

The effectiveness of carbon coating in improving the electrochemical performances of the substrate materials is affected by many factors: the weight ratio, conductivity, thickness, coating uniformity, *etc*. A much low carbon content cannot satisfy full coating and enough conductivity, a too high content leads to a low electrode density. The conductivity of the carbon coating layer strongly depends on the thermal treatment temperature and carbon sources. Low temperature produces amorphous carbon with low conductivity; while high temperature helps to get good conductivity but leads to a high risk of the reduction of the substrate materials. For example, J. D. Wilcox *et al.* systematically studied the structural factors of the carbon coating layers obtained with different carbon sources, carbon content and coating procedures by Raman spectroscopy and elemental analysis.[18] They pointed out that the quality of carbon coatings, such as sp^2/sp^3 ratio, disordered/graphitic ratio, and H/C ratio, would strongly influence the conductivity and rate behavior of the $LiFePO_4$/C composite. The more graphitic carbon coatings with better homogeneously coverage, even with a low carbon content ($<$2 wt%), would result in higher pressed-pellet conductivities of the $LiFePO_4$/C composites and improved electrochemical performances of cells containing these materials. The control of the carbon coating thickness is also a challenge in practical synthesis procedures. A low amount of carbon source might form a thin but hardly a full coating layer on the surface of substrate; while a too thick carbon coating layer would act as a barrier for Li^+ diffusion. The study of R. Dominko showed that when the carbon coating thickness was increased from 1 nm to 10 nm, both the bulk density of $LiFePO_4$/C composite and its reversible capacity decreased, which are due to the increasingly hindered electrolyte transport and increased amount of Fe(III) species.[19]

Among the frequently-used coating technologies, mechanical methods such as dry/wet mixing by ball milling or grinding are most convenient and are of low cost to implement, and thus are easy to scale up in commercial view. However, it is difficult to obtain a full and uniform coating layer. Strictly speaking, they lead to a distribution of carbon in the active material rather than a carbon coating layer on the surface of active material. The pre-addition of a dissolved carbon precursor in course of synthesis followed by post-carbonization in heat treatment provides high operation flexibility, *e.g.* wide adaptivity to substrate material, abundant carbon sources, adjusted concentration, smart adding procedure *etc*., and thus has been used for many materials and demonstrated unique advantages especially in nanostructure related fields. However, the synthesis routes are relatively complex and time-consuming, and sensitive to many experiment parameters. The coating quality and structure features of the final products are critically related to the used synthesis conditions and strategy. Chemical or thermal vapor deposition technologies favor uniform and full coating of carbon with high conductivity, and are feasible to control the coating thickness and carbon content. However, they have to be carried out in inert gas flow and at high temperature, thus is of high cost and is high energy-consuming. In a word, there should be an ongoing effort to develop a simple and low cost method to achieve a high quality carbon coating layer with good uniformity, thin thickness and high conductivity.

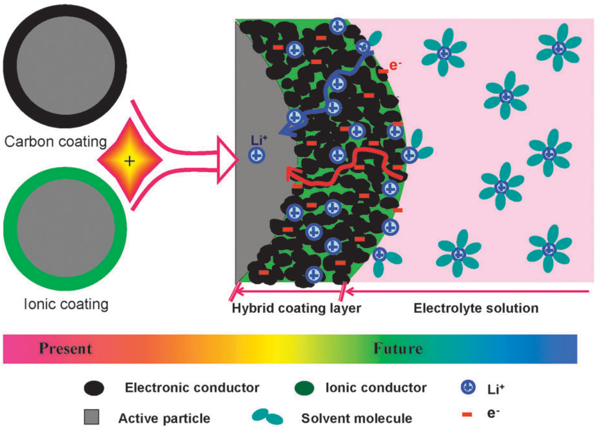

Fig. 15 Schematic illustration of the "electronic and ionic hybrid coating layer" for the active electrode material during charge/discharge processes.

5.3 "Hybrid coatings" for future development

In fact, the charge and discharge process of an electrode would involve a series of complex chemical and physical procedures at the interface of electrode/electrolyte. An ideal coating layer for the electrode material should play multi-functional roles. It should be highly conductive for both Li^+ and electrons, should facilitate easy solvation/desolvation of Li^+, favor a fast formation of thin and compact SEI, and provide reliable protection against HF attack, *etc*. However, it is not possible to find such a panacea in the existing coating materials. Instead, the combination of different coating materials, *e.g.*, to build a "hybrid coating layer", might be an alternative in the next stage, as shown in Fig. 15. Carbon shows excellent electronic conductivity among the reported coating materials, but it is not a good ionic conductor. Lithium phosphates are well known as good and stable Li^+ conductors and their coating on $LiFePO_4$ has demonstrated a great improvement in the rate performance.[81] Besides, Li_3PO_4 was also found to be an effective SEI when coated on the surface of a $LiNi_{0.5}Mn_{1.5}O_4$ spinel to prevent the degradation of the electrolyte.[82] If carbon and lithium phosphate can be co-coated on the surface of the active particles, the obtained hybrid coating layer would provide both high electronic and ionic conductivity for the core active material. Other functional components such as metal oxides (HF scavenger) and metal fluoride (physical protector) can also be added in the hybrid coating layer. Such a hybrid coating layer might be a promising surface coating technique in the near future.

6. Conclusion

Surface carbon coating can be easily achieved with low cost by thermal decomposition of various precursors or chemical vapor deposition technique in an inert atmosphere. It has been applied for a wide range of electrode materials and exhibited impressive advances in improving the electrochemical performances of both cathodes and anodes especially as $LiMPO_4$ and graphite electrodes. Attributed to its excellent electrical conductivity, superior chemical/electrochemical stability, and unique physical properties, the carbon coating layer can behave as a multi-functional layer between the active electrode and electrolyte to enhance the electrode conductivity, reduce the surface activity of nanomaterial, improve the SEI film, protect the active material from electrolyte corrosion, and maintain the electrode integration and conductivity upon volume change, thus resulting in much improved rate capability and cycle stability of the coated materials. It can also serve as a dimension restrictor to prevent the nanoparticles from aggregating and growing, thus maintaining the nanostructure morphology. However, ongoing effort should be made to develop new coating techniques to overcome its limitation in application for lithium transition metal oxides and shortcoming in ionic conductivity.

References

1 J. M. Tarascon, *Philos. Trans. R. Soc. London, Ser. A*, 2010, **368**, 3227–3241.
2 A. Manthiram, *J. Phys. Chem. Lett.*, 2011, **2**, 176–184.
3 R. Marom, S. F. Amalraj, N. Leifer, D. Jacob and D. Aurbach, *J. Mater. Chem.*, 2011, **21**, 9938–9954.
4 J. M. Tarascon and M. Armand, *Nature*, 2001, **414**, 359–367.
5 C. Li, H. P. Zhang, L. J. Fu, H. Liu, Y. P. Wu, E. Rahm, R. Holze and H. Q. Wu, *Electrochim. Acta*, 2006, **51**, 3872–3883.
6 L. J. Fu, H. Liu, C. Li, Y. P. Wu, E. Rahm, R. Holze and H. Q. Wu, *Solid State Sci.*, 2006, **8**, 113–128.
7 S. T. Myung, K. Amine and Y. K. Sun, *J. Mater. Chem.*, 2010, **20**, 7074–7095.
8 Z. Chen, Y. Qin, K. Amine and Y. K. Sun, *J. Mater. Chem.*, 2010, **20**, 7606–7612.
9 M. Park, X. Zhang, M. Chung, G. B. Less and A. M. Sastry, *J. Power Sources*, 2010, **195**, 7904–7929.
10 M. Gaberscek, R. Dominko and J. Jamnik, *Electrochem. Commun.*, 2007, **9**, 2778–2783.
11 P. G. Bruce, B. Scrosati and J. M. Tarascon, *Angew. Chem., Int. Ed.*, 2008, **47**, 2930–2946.
12 Y. Wang, H. Li, P. He, E. Hosono and H. Zhou, *Nanoscale*, 2010, **2**, 1294–1305.
13 C. M. Julien, *J. Appl. Phys.*, 2006, **100**, 063511.
14 W. Zhang, J. Hu, Y. Guo, S. Zheng, L. Zhong, W. Song and L. Wan, *Adv. Mater.*, 2008, **20**, 1160–1165.
15 A. S. Andersson and J. O. Thomas, *J. Power Sources*, 2001, **97–98**, 498–502.
16 J. M. Tarascon, C. Delacourt, A. S. Prakash, M. Morcrette, M. S. Hegde, C. Wurm and C. Masquelier, *Dalton Trans.*, 2004, 2988–2994.
17 X. Zhi, G. Liang, L. Wang, X. Ou, L. Gao and X. Jie, *J. Alloys Compd.*, 2010, **503**, 370–374.
18 J. D. Wilcox, M. M. Doeff, M. Marcinek and R. Kostecki, *J. Electrochem. Soc.*, 2007, **154**, A389–A395.
19 R. Dominko, M. Bele, M. Gaberscek, M. Remskar, D. Hanzel, S. Pejovnik and J. Jamnik, *J. Electrochem. Soc.*, 2005, **152**, A607–A610.
20 Y. D. Cho, G. T. K. Fey and H. M. Kao, *J. Power Sources*, 2009, **189**, 256–262.
21 Y. Wang, Y. Wang, E. Hosono, K. Wang and H. Zhou, *Angew. Chem., Int. Ed.*, 2008, **47**, 7461–7465.
22 X. Zhou, F. Wang, Y. Zhu and Z. Liu, *J. Mater. Chem.*, 2011, **21**, 3353–3358.
23 K. Amine, J. Liu and I. Belharouak, *Electrochem. Commun.*, 2005, **7**, 669–673.
24 S. W. Oh, S. T. Myung, S. M. Oh, K. H. Oh, K. Amine, B. Scrosati and Y. K. Sun, *Adv. Mater.*, 2010, **22**, 4842–4845.
25 J. F. Martin, A. Yamada, G. Kobayashi, S. I. Nishimura, R. Kanno, D. Guymard and N. Dupre, *Electrochem. Solid-State Lett.*, 2008, **11**, A12–A16.
26 G. Kobayashi, S. I. Nishimura, M. S. Park, R. Kanno, M. Yashima, T. Ida and A. Yamada, *Adv. Funct. Mater.*, 2009, **19**, 395–403.
27 Y. Wang, P. He and H. Zhou, *Energy Environ. Sci.*, 2011, **4**, 805–817.
28 J. Yang and J. J. Xu, *J. Electrochem. Soc.*, 2006, **153**, A716–A723.
29 A. Yamada, Y. Kudo and K. Y. Liu, *J. Electrochem. Soc.*, 2001, **148**, A747–A754.
30 M. Yonemura, A. Yamada, Y. Takei, N. Sonoyama and R. Kanno, *J. Electrochem. Soc.*, 2004, **151**, A1352–A1356.
31 T. N. L. Doan, Z. Bakenov and I. Taniguchi, *Adv. Powder Technol.*, 2010, **21**, 187–196.
32 S. M. Oh, S. W. Oh, C. S. Yoon, B. Scrosati, K. Amine and Y. K. Sun, *Adv. Funct. Mater.*, 2010, **20**, 3260–3265.
33 S. K. Martha, J. Grinblat, O. Haik, E. Zinigrad, T. Drezen, J. H. Miners, I. Exnar, A. Kay, B. Markovsky and D. Aurbach, *Angew. Chem., Int. Ed.*, 2009, **48**, 8559–8563.
34 A. M. Hashem, A. E. A. Ghany, K. Nikolowski and H. Ehrenberg, *Ionics*, 2010, **16**, 305–310.
35 B. L. Cushing and J. B. Goodenough, *Solid State Sci.*, 2002, **4**, 1487–1493.
36 H. S. Kim, M. Kong, K. Kim, I. J. Kim and H. B. Gu, *J. Power Sources*, 2007, **171**, 917–921.
37 R. Guo, P. Shi, X. Cheng and C. Du, *J. Alloys Compd.*, 2009, **473**, 53–59.
38 H. S. Kim, K. Kim, S. I. Moon, I. J. Kim and H. B. Gu, *J. Solid State Electrochem.*, 2008, **12**, 867–872.
39 B. Lin, Z. Wen, X. Wang and Y. Liu, *J. Solid State Electrochem.*, 2010, **14**, 1807–1811.
40 M. L. Marcinek, J. W. Wilcox, M. M. Doeff and R. M. Kostecki, *J. Electrochem. Soc.*, 2009, **156**, A48–A51.
41 M. M. Thackeray, S. H. Kang, C. S. Johnson, J. T. Vaughey, R. Benedek and S. A. Hackney, *J. Mater. Chem.*, 2007, **17**, 3112–3125.
42 J. Liu and A. Manthiram, *Chem. Mater.*, 2009, **21**, 1695–1707.
43 J. Liu, A. Wang, B. Reeja-Jayan and A. Manthiram, *Electrochem. Commun.*, 2010, **12**, 750–753.
44 K. Zaghib, M. Simoneau, M. Armand and M. Gauthier, *J. Power Sources*, 1999, **81–82**, 300–305.
45 C. H. Chen, J. T. Vaughey, A.N. Jansen, D. W. Dees, A. J. Kahaian, T. Goacher and M. M. Thackeray, *J. Electrochem. Soc.*, 2001, **148**, A102–A104.
46 T. Doi, Y. Iriyama, T. Abe and Z. Ogumi, *Chem. Mater.*, 2005, **17**, 1580–1582.
47 L. Cheng, H. J. Liu, J. J. Zhang, H. M. Xiong and Y. Y. Xia, *J. Electrochem. Soc.*, 2006, **153**, A1472–A1477.
48 Y. Li, G. L. Pan, J. W. Liu and X. P. Gao, *J. Electrochem. Soc.*, 2009, **156**, A495–A499.
49 E. M. Sorensen, S. J. Barry, H. K. Jung, J. R. Rondinelli, J. T. Vaughey and K. R. Poeppelmeier, *Chem. Mater.*, 2006, **18**, 482–489.
50 L. Zhao, Y. S. Hu, H. Li, Z. Wang and L. Chen, *Adv. Mater.*, 2011, **23**, 1385–1388.
51 L. Cheng, X. L. Li, H. J. Liu, H. M. Xiong, P. W. Zhang and Y. Y. Xia, *J. Electrochem. Soc.*, 2007, **154**, A692–A697.
52 J. Wang, X. M. Liu, H. Yang and X. D. Shen, *J. Alloys Compd.*, 2011, **509**, 712–718.
53 T. Yuan, X. Yu, R. Cai, Y. Zhou and Z. Shao, *J. Power Sources*, 2010, **195**, 4997–5004.

54 H. Liu, Y. Feng, K. Wang and J. Xie, *J. Phys. Chem. Solids*, 2008, **69**, 2037–2040.

55 Y. Wang, H. Liu, K. Wang, H. Eiji, Y. Wang and H. Zhou, *J. Mater. Chem.*, 2009, **19**, 6789–6795.

56 L. Cheng, J. Yan, G. N. Zhu, J. Y. Luo, C. X. Wang and Y. Y. Xia, *J. Mater. Chem.*, 2010, **20**, 595–602.

57 M. Yoshio, H. Wang, K. Fukuda, T. Umeno, T. Abe and Z. Ogumi, *J. Mater. Chem.*, 2004, **14**, 1754–1758.

58 C. Natarajan, H. Fujimoto, K. Tokumitsu, A. Mabuchi and T. Kasuh, *Carbon*, 2001, **39**, 1409–1413.

59 H. L. Zhang, S. H. Liu, F. Li, S. Bai, C. Liu, J. Tan and H. M. Cheng, *Carbon*, 2006, **44**, 2212–2218.

60 Y. S. Han and J. Y. Lee, *Electrochim. Acta*, 2003, **48**, 1073–1079.

61 M. Yoshio, H. Wang, K. Fukuda, Y. Hara and Y. Adachi, *J. Electrochem. Soc.*, 2000, **147**, 1245–1250.

62 H. Wang, M. Yoshio, T. Abe and Z. Ogumi, *J. Electrochem. Soc.*, 2002, **149**, A499–A503.

63 H. Wang and M. Yoshio, *J. Power Sources*, 2001, **93**, 123–129.

64 M. Yoshio, H. Wang and K. Fukuda, *Angew. Chem., Int. Ed.*, 2003, **42**, 4203–4206.

65 Y. S. Park, H. J. Bang, S. M. Oh, Y. K. Sun and S. M. Lee, *J. Power Sources*, 2009, **190**, 553–557.

66 M. Yoshio, H. Wang, K. Fukuda, T. Umeno, N. Dimov and Z. Ogumi, *J. Electrochem. Soc.*, 2002, **149**, A1598–A1603.

67 N. Domov, K. Fukuda, T. Umeno, S. Kugino and M. Yoshio, *J. Power Sources*, 2003, **114**, 88–95.

68 Y. Qiu, K. Yan and S. Yang, *Chem. Commun.*, 2010, **46**, 8359–8361.

69 Y. Li, X. Lv, J. Lu and J. Li, *J. Phys. Chem. C*, 2010, **114**, 21770–21774.

70 R. Yang, W. Zhao, J. Zheng, X. Zhang and X. Li, *J. Phys. Chem. C*, 2010, **114**, 20272–20276.

71 G. X. Wang, J. H. Ahn, J. Yao, S. Bewlay and H. K. Liu, *Electrochem. Commun.*, 2004, **6**, 689–692.

72 S. H. Ng, J. Wang, D. Wexler, S. Y. Chew and H. K. Liu, *J. Phys. Chem. C*, 2007, **111**, 11131–11138.

73 Y. J. Kwon and J. Cho, *Chem. Commun.*, 2008, 1109–1111.

74 X. W. Lou, J. S. Chen, P. Chen and L. A. Archer, *Chem. Mater.*, 2009, **21**, 2868–2874.

75 W. J. Cui, F. Li, H. J. Liu, C. X. Wang and Y. Y. Xia, *J. Mater. Chem.*, 2009, **19**, 7202–7207.

76 Y. H. Xu, G. P. Yin, Y. L. Ma, P. J. Zuo and X. Q. Cheng, *J. Mater. Chem.*, 2010, **20**, 3216–3220.

77 K. Kang, K. Song, H. Heo, S. Yoo, G. S. Kim, G. Lee, Y. M. Kang and M. H. Jo, *Chem. Sci.*, 2011, **2**, 1090–1093.

78 K. T. Lee, Y. S. Jung and S. M. Oh, *J. Am. Chem. Soc.*, 2003, **125**, 5652–5653.

79 X. W. Lou, D. Deng, J. Y. Lee and L. A. Archer, *Chem. Mater.*, 2008, **20**, 6562–6566.

80 Y. S. Lin, J. G. Cuh and M. H. Hung, *J. Phys. Chem. C*, 2010, **114**, 13136–13141.

81 B. Kang and G. Ceder, *Nature*, 2009, **458**, 190–193.

82 Y. Kobayashi, H. Miyashiro, K. Takei, H. Shigemura, M. Tabuchi, H. Kageyama and T. Iwahoria, *J. Electrochem. Soc.*, 2003, **150**, A1577–A1582.